Colloidal Brownian motion in corrugated channels: When hydrodynamic interactions hamper entropic diffusion

Xiang Yang,[1] Chang Liu,[1] Yunyun Li,[2] Fabio Marchesoni,[2,3] Peter Hänggi,[4,5] and H. P. Zhang[1,6,*]

[1] *Department of Physics and Astronomy and Institute of Natural Sciences, Shanghai Jiao Tong University, Shanghai 200240, China*
[2] *Center for Phononics and Thermal Energy Science, School of Physics Science and Engineering, Tongji University, Shanghai 200092, China*
[3] *Dipartimento di Fisica, Universit?i Camerino, I-62032 Camerino, Italy*
[4] *Institut für Physik, Universität Augsburg, D-86135 Augsburg, Germany*
[5] *Nanosystems Initiative Munich, Schellingstrasse 4, D-80799 München, Germany*
[6] *Collaborative Innovation Center of Advanced Microstructures, Nanjing 210093, China*

(Dated: May 8, 2017)

Confined diffusion characterizes transport in many natural and artificial devices, such as ionic channels, zeolites, and nanopores. While this important subject has been extensively studied analytically and by numerical simulations, systematic experimental investigations are rare. Here, we experimentally measure colloidal diffusion times in microchannels with periodically varying width and contrast results with predictions from the Fick-Jacobs theory and Brownian dynamics simulation. While the theory and simulation correctly predict the entropic effect of the varying channel width, they fail to account for hydrodynamic effects, which include both an overall decrease and a spatial variation of diffusivity in channels. Neglecting such hydrodynamic effects, the theory and simulation underestimate the mean and standard deviation of first passage times by 40% in channels with a neck width twice the particle diameter. We further show that the validity of the Fick-Jakobs theory can be restored by reformulating it in terms of the experimentally measured diffusivity. Our work thus demonstrates that hydrodynamic effects play a key role in diffusive transport through narrow channels.

Diffusive transport occurs prevalently in confined geometries [1, 2]. Notable examples include the dispersion of tracers in permeable rocks [3], diffusion of chemicals in ramified matrices [4], and the motion of submicron corpuscles in living tissues [5, 6]. Spatial confinement can fundamentally change equilibrium and dynamical properties of a system by both limiting the configuration space accessible to its diffusing components [1] and increasing the hydrodynamic drag [7] on them. The subject of confined diffusion is of paramount relevance to technological applications and for this reason has been attracting growing interest in the physics [1, 2], mathematics [8], engineering [3], and biology communities [5, 6, 9].

From a theoretical point of view, particle diffusion in a confining structure can be formulated in terms of a high dimensional Fokker-Planck equation with appropriate boundary conditions reproducing the structure's geometry. Such a boundary value problem is difficult to treat in general. However, an approximate approach allows circumventing this difficulty in the case of quasi-1D structures, such as ionic channels [10], zeolites [4], micro-fluidic channels [11, 12], and nanopores [13]. In these systems, transport takes place along a preferred direction with the spatial constraints varying along it. A typical example is represented by a corrugated narrow channel. Focusing on the transport direction, Jacobs [14] and Zwanzig [15] assumed that the transverse degrees of freedom equilibrate fast and proposed to eliminate them adiabatically by means of an approximate perturbation scheme. In first order, they derived a reduced diffusion equation, known as Fick-Jacobs (FJ) equation, reminiscent of an ordinary 1D Fokker-Planck equation *in vacuo*, except for two entropic terms, which locally modify the drift and diffusion properties of the channeled particle [2, 16–19].

The FJ equation can be analytically solved to determine relevant transport quantifiers, such as the effective mobility and diffusivity along the channel. The theoretical predictions of the FJ reductionist approach have been extensively checked against Brownian dynamics (BD) simulations, which, on the contrary, propose to numerically integrate the full multi-dimensional Langevin equation describing diffusion in arbitrary geometries. Different types of channels have been investigated, including 2D [16, 20, 21] and 3D channels [19, 22, 23], channels with abruptly changing cross-sections [23, 24], and curved channels [25–27]. On combining theoretical and computational techniques, a variety of novel entropy-driven transport mechanisms have been predicted, such as drive-dependent mobilities [2, 18, 20], stochastic resonance [28, 29], absolute negative mobilities [30], entropic rectification [31, 32], and particle separation [33]. Several of these results are presently recognized as being of both fundamental and technological importance.

Surprisingly, experimental studies of entropic effects on confined diffusion are still scarce [12, 34–36], mainly due to technical difficulties encountered in fabricating micron-sized corrugated channels of controlled width [37]. Here, we implemented a two-photon direct laser writing technique to overcome this experimentally difficult prob-

lem and fabricated channels with systematically modulated cross-sections. We then measured the diffusive dynamics of micrometric colloidal particles through such channels by standard video microscopy and compared the outcome with predictions obtained by FJ approximation and from BD simulation. We discover that, as the channel's width shrinks towards the particle's diameter, hydrodynamic effects [7, 38–42], largely ignored in previous studies, grow in strength and become comparable to the predicted entropic effects, thus indicating an unexpected breakdown of the standard FJ theory and BD simulation in narrow channels. We further show that hydrodynamic effects can be incorporated by using an experimentally measured local diffusivity. With such a phenomenological modification, the FJ theory and BD simulation accurately predict the experimental data.

RESULTS

Experimental realization

Our channels were fabricated on a cover slip by means of a two-photon direct laser writing system, which solidifies polymers according to the preassigned channel profile, $f(x)$, with a sub-micron resolution. As shown in Fig. 1, the quasi-two-dimensional channel has a uniform height of 2.5μm (z direction). The curved side walls are 0.7μm thick and their inner side walls a distance $\pm h(x)$ away from the channel's axis (x direction).

After fabrication, channels were immersed in water with fluorescently-labeled Polystyrene spheres of radius $r = 0.5\mu$m. A holographic optical tweezer was used to drag a particle into the channel through a narrow entrance [red symbols in Fig. 1(a)]. The entrances are barely wider than the particle diameter so as to create insurmountable entropic barriers [2], which prevent the particle inside the channel from escaping. Particle motion in the quasi-two-dimensional channel was recorded through a microscope at rate of 30 frame/sec for up to 20 hours. The projected particle trajectory in xy plane was extracted from the recorded videos by standard particle tracking algorithms; particle diffusion perpendicular to the imaging xy plane was not resolved in our measurements.

Inside the channels, the particle diffuses in a flat energy landscape. To show that, we quantized the measured particle coordinates (x, y) into small bins (0.4×0.25 μm^2) and counted the number of times the particle enters each bin. As shown in Fig. 1(b), particle counts are uniformly distributed with a standard variation about 12% of the mean. Regions where the particle counts drop sharply to zero are inaccessible to the particle's center and, in Fig. 1(b), are delimited by the black curves [see also the inset of Fig. 2(a)]. The effective channel's boundary [denoted by $g(x)$] is a periodic function; in the central region, the boundary was given the form of a cosine, which then tapers off to a constant in correspondence with the bottlenecks, that is

$$g(x) = \begin{cases} \frac{1}{2}(g_w + g_n) + \frac{1}{2}(g_w - g_n)\cos(\frac{16\pi x}{7L}), & |x| < \frac{7}{16}L \\ g_n, & \frac{7}{16}L \le |x| \le \frac{L}{2} \end{cases} \quad (1)$$

The length of the channel unit cell was kept fixed in all experiments, $L = 12.5\mu$m, while the parameters g_n and g_w, representing respectively, its minimum and maximum half-width, were varied. For the channel shown in Fig. 1(b), $g_n = 0.5\mu$m, and $g_w = 4.5\mu$m.

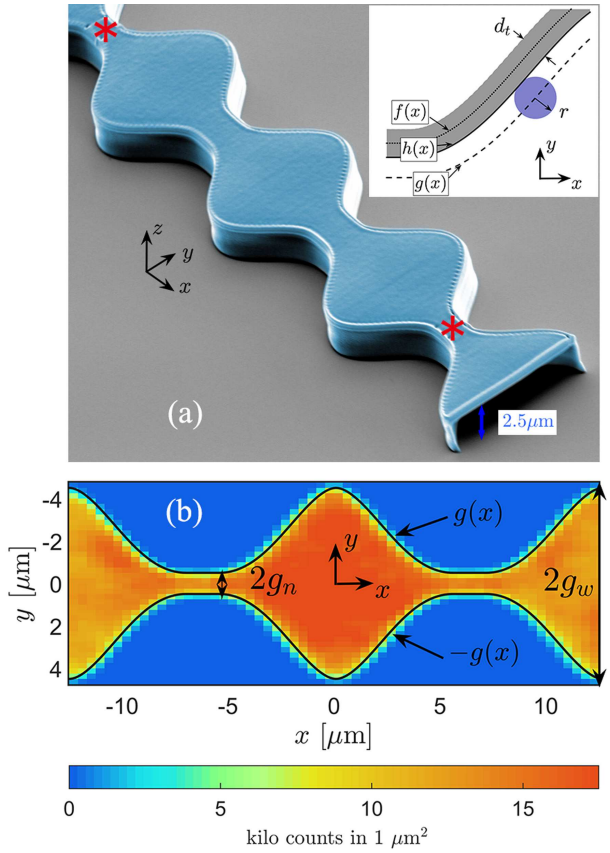

Figure 1. | **Channel geometry.** (**a**) Scanning electron image of a channel of inner height 2.5μm. Narrow openings at the two ends are marked by red symbols. The inset illustrates the channel's geometry: the laser scanning contour, $f(x)$, the wall inner boundary, $h(x)$, and the effective boundary of the space accessible to the particle center, $g(x)$; $d_t \simeq 0.7\mu$m and $r = 0.5\mu$m are the wall thickness and the particle radius, respectively. (**b**) Spatial distribution of particle counts in a typical 20-hour-long experiment. The effective channel boundary is marked by black lines and is denoted by $\pm g\,(x)$, see Eq. (1); here, $g_n = 0.5\mu$m, and $g_w = 4.5\mu$m.

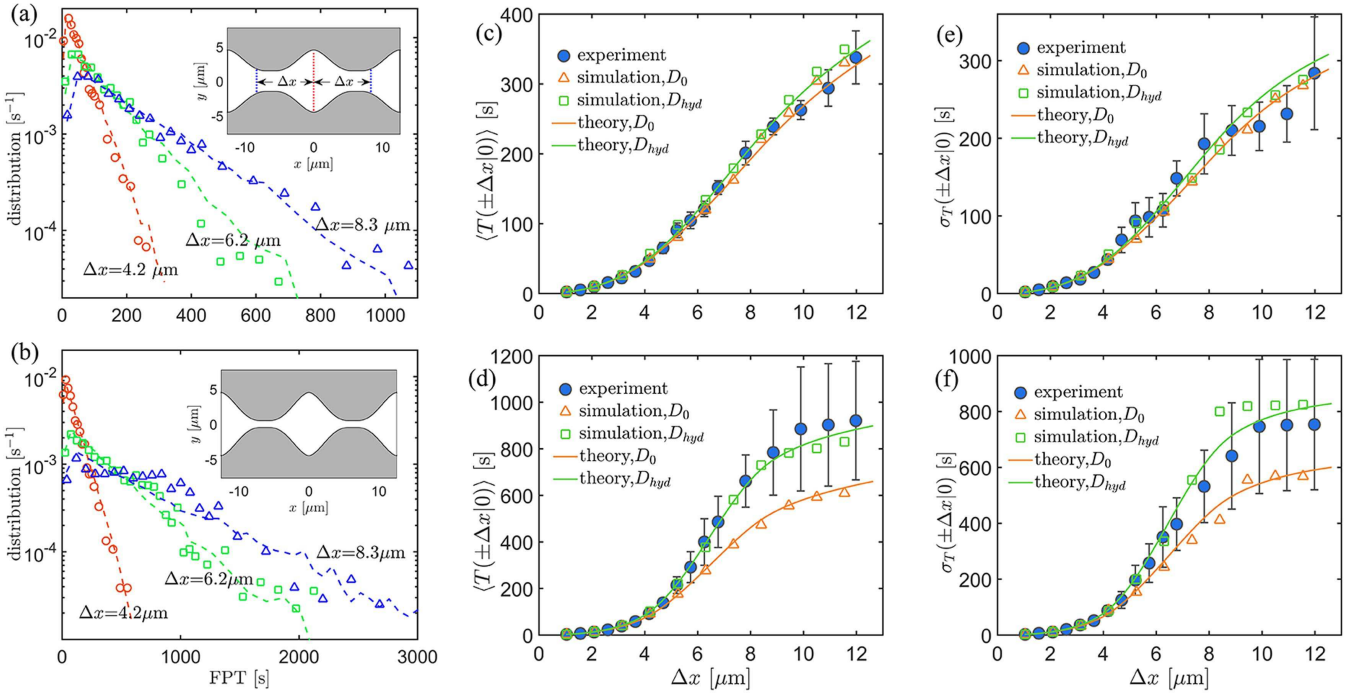

Figure 2. | **Statistics of the first passage times.** Probability distributions, (**a**, **b**), averages, (**c**, **d**), and standard deviations, (**e**, **f**) of the FPT's in a wide (top row, $g_n = 1.5\mu$m) and narrow (bottom row, $g_n = 0.5\mu$m) channel with same maximum half-width, $g_w = 4.5\mu$m. In (**a**, **b**), experimental data (symbols) are compared with the outcome of Brownian dynamics simulations (curves) for the spatially modulated diffusivity, $D_{hyd}(x)$. The relevant channel profiles, $\pm g(x)$, are shown in the insets of (**a**, **b**); vertical dashed segments mark the starting (red, $x = 0$) and ending (blue, $x = \pm\Delta x$) positions of the first passage events. In (**c-f**), experimental, numerical, and theoretical results are shown as solid symbols, empty symbols, and solid curves, respectively. Numerical and theoretical results with constant, D_0, and varying, D_{hyd}, diffusivity are color coded, respectively, in orange and green.

First passage time statistics

A direct measurement of the diffusion constant in channels [1], $D_c = \lim_{t\to\infty}\langle[x(t) - x(0)]^2\rangle/(2t)$, would require fabricating a much longer (linear or circular) channel structure. As a more viable alternative we measured the First Passage Times (FPT) [8, 43, 44]. As in the FJ theory, we focus on the particle motion along the channel direction and measure the duration of the unconditional first passage events that start at $x = 0$ [red segment in the inset of Fig. 2(a)] and end at $x = \pm\Delta x$ (blue segments), with no restriction on the transverse coordinate y. Distributions of experimentally measured unconditional FPTs, also denoted by $T(\pm\Delta x|0)$, are plotted in Figs. 2(a,b); all distributions (for three Δx values in two channels of different bottleneck half-width, g_n) exhibit an exponential tail, similar in spirit with the narrow-escape problem [8]. From these measured FPT distributions, we extract the means, $\langle T(\pm\Delta x|0)\rangle$, and the standard deviations, $\sigma_T(\pm\Delta x|0) := \sqrt{\langle T^2(\pm\Delta x|0)\rangle - \langle T(\pm\Delta x|0)\rangle^2}$; our results are plotted in Figs. 2(c-f) against the diffusing distance, Δx. A decrease of the bottleneck width, g_n, from 1.5μm in (c) to 0.5μm in (d), sharply increases the diffusion time. For instance, the mean FPT to the center of the adjacent cells, $\langle T(\pm L|0)\rangle$, nearly triples from 300s in (c) to 900s in (d). A similar increase can be observed in the standard deviations, $\sigma_T(\pm\Delta x|0)$, depicted in Figs. 2(e,f). To this regard, we notice that, for both channels, the experimental curves $\langle T(\pm\Delta x|0)\rangle$ and $\sigma_T(\pm\Delta x|0)$, almost overlap, as to be expected in view of the exponential decay of the relevant FPT distributions [44]. Accordingly, the corresponding channel diffusion constant, D_c, can be estimated in terms of an appropriate mean FPT; that is [44], $D_c = L^2/(2\langle T(\pm L|0)\rangle)$.

We next compare our experimental data with the predictions of the standard FJ theory and BD simulations. The channel geometry renders our experimental system effectively two-dimensional; analytical and numerical studies were carried out in the same dimension. Following the FJ scheme and taking advantage of symmetry properties of our experiments, we calculate the analytical expression,

$$\langle T_{FJ}(\pm\Delta x|0)\rangle = \int_0^{\Delta x} \frac{d\eta}{g(\eta)\mathbb{D}(\eta)} \int_0^{\eta} g(\xi)d\xi, \qquad (2)$$

for the mean FPT. Here, $\mathbb{D}(x)$ is the effective local diffusivity containing the entropic corrections that result from the adiabatic elimination of the transverse coordi-

nate, y. Among the (slightly) different functions $\mathbb{D}(x)$ proposed in the recent literature [21], we adopted the Reguera-Rubì heuristic expression [16], i.e.,

$$\mathbb{D}(x) = \frac{D_0}{[1+g'(x)^2]^{1/3}}, \tag{3}$$

where $g'(x)$ is the slope of the channel's profile $g(x)$, and D_0 is the particle's diffusivity away from side walls. We also calculated the second FPT moment,

$$\langle T_{FJ}^2(\pm\Delta x|0)\rangle = \int_0^{\Delta x} \frac{2d\eta}{g(\eta)\mathbb{D}(\eta)} \int_0^{\eta} g(\xi)\langle T_{FJ}(\pm\Delta x|\xi)\rangle d\xi, \tag{4}$$

where $\langle T_{FJ}(\pm\Delta x|\xi)\rangle$ reads like in Eq. (2), except that the outer integral runs here from ξ to Δx. The derivation of Eqs. (2) and (4) can be found in the Supplementary Information (SI).

To use Eqs. (2) to (4), we need to know the diffusivity, D_0. Unlike in an unbounded space, where the diffusivity of a sphere is determined by the Stokes-Einstein equation, there is no general expression for the diffusivity of a colloidal particle in a confined geometry. Hence, we experimentally measured D_0 by monitoring the diffusion of the particle about the center of a channel's cell, where the entropic effects are minimal, and for displacements smaller than one particle radius. The FJ expressions (2) and (4) were then computed explicitly for the measured value of D_0 and the actual channel geometry (namely, the parameters g_n, g_w, and L). For the sake of a comparison, 2D BD simulations were also performed for the same model parameters. Theoretical and numerical results, orange symbols and curves in Fig. 2(c-f), agree closely with each other for both the wide and narrow channel. The comparison with the experimental data, instead, is satisfactory only in the case of the wide channel, Figs. 2(c, e). For the narrow channel of Figs. 2 (d, f), the experimental data with $\Delta x > 6\mu$m are as much as 40% larger than the predicted values. To further investigate this discrepancy, we carried out experiments in channels with different width parameters, g_w and g_n; the discrepancy is quantified in Fig. 3 by the relative mean-FPT difference at $\Delta x = L/2$ (bottleneck midpoints), $E_{FJ} = [\langle T(\pm L/2|0)\rangle - \langle T_{FJ}(\pm L/2|0)\rangle]/\langle T_{FJ}(\pm L/2|0)\rangle$. For narrow channels, the experimental data are consistently larger than the corresponding theoretical and numerical predictions. The discrepancy depends weakly on the amplitude of the channel modulation, $g_w - g_n$, but increases significantly with decreasing bottleneck half-width, g_n.

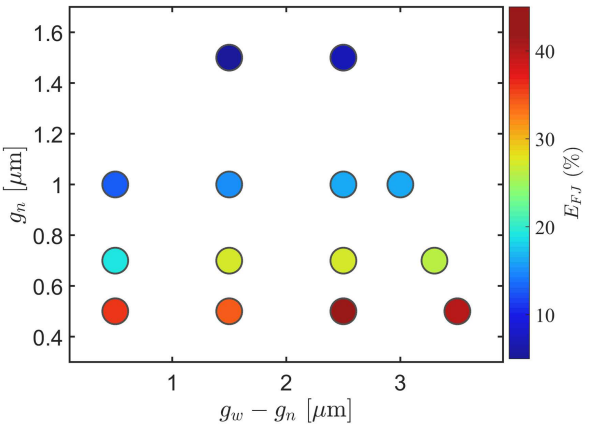

Figure 3. | **Deviation of theoretical predictions from experimental results.** Relative deviation, E_{FJ}, increases with decreasing the bottleneck half-width, g_n, and weakly depends on the modulation amplitude, $g_w - g_n$, of the channel.

Diffusivity measurements

The theoretical and numerical predictions discussed so far assume a constant particle diffusivity, D_0, throughout the channel, which is a reasonable approximation for particle diameters much smaller than the channel width. However, this assumption is doomed to fail for small bottleneck widths (when the FJ approach is supposed to work best), because the proximity of no-slip side walls in the neck regions is known to increase the hydrodynamic drag on a finite-size particle and, therefore, suppress its local diffusivity [39–42, 45, 46].

To demonstrate such a hydrodynamic effect in our device, we measured the particle diffusivity inside the channel. At any given location, (x, y), we recorded the particle mean-squared displacement in the x direction, $\langle \delta x^2(x,y)\rangle$, for a time interval $\delta t = 0.2$s and estimated the local diffusivity through Einstein's law, $D(x,y) = \langle \delta x^2(x,y)\rangle / (2\delta t)$. As shown in SI, the value chosen for δt is long enough to ensure a good statistics for our measurements of $D(x,y)$, but not enough for the entropic effects and spatial variability of $D(x,y)$ due to the channel modulation to become detectable. Measurements of $D(x,y)$ in the wide and narrow channels are shown in Fig. 4(a, b). In both, $D(x,y)$ is largest in the open regions at the center of the unit cells, and strongly suppressed in the bottlenecks. In the spirit of the FJ theory, we average $D(x,y)$ along the transverse direction

$$D_{hyd}(x) \coloneqq \frac{1}{2g(x)} \int_{-g(x)}^{g(x)} D(x,y)dy \tag{5}$$

and plot $D_{hyd}(x)/D_0$ as a function of x in Fig. 4(c). The spatial variability of $D_{hyd}(x)$ is about 10% and 40% for the wide and narrow channels, respectively.

We corroborate the local diffusivity measurements with full hydrodynamic computations. The hydrodynamic friction coefficient in the x direction $\gamma(x,y)$ was computed by means of a finite-element package (COMSOL); the local diffusivity was calculated via the

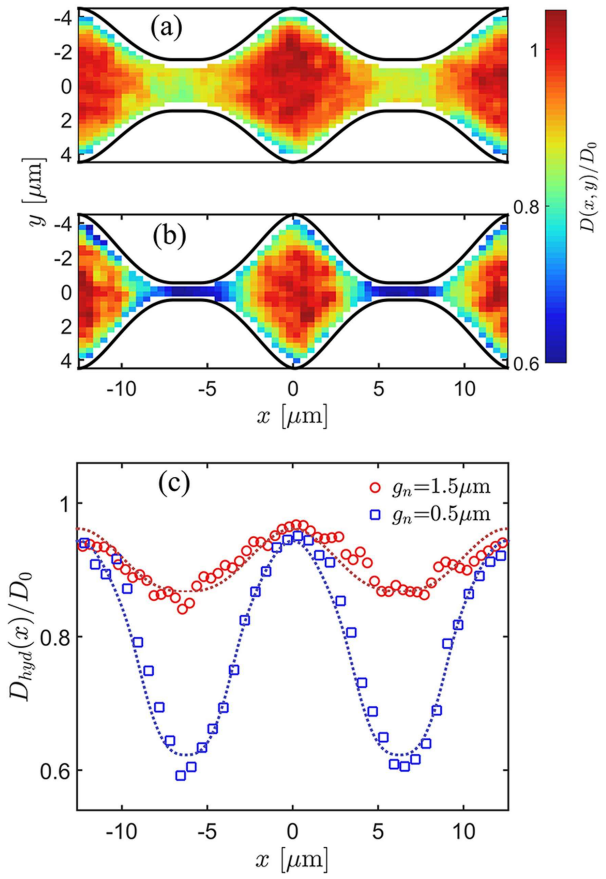

Figure 4. | **Spatial variability of the local diffusivity.** (**a**, **b**) Normalized diffusivity from experiments, $D(x,y)/D_0$, measured in the wide and narrow channels of Fig. 2. (**c**) Normalized diffusivity, $D_{hyd}(x)/D_0$, versus x. Experimental data and results from finite-element calculations are represented respectively by symbols and curves. Experimentally measured D_0 is 0.29 μm^2/s and 0.27 μm^2/s for wide and narrow channels, respectively; the Stokes-Einstein equation predicts a sphere diffusivity of 0.5 μm^2/s in an unbounded space.

fluctuation-dissipation theorem, $D(x,y) = k_BT/\gamma(x,y)$, and the result is averaged over the y coordinate to obtain $D_{hyd}(x)$. Results from finite-element calculations are shown in Fig. 4(c) as curves and are in excellent agreement with the experimental data.

Hydrodynamic correction

Figure 4 depicts that particle diffusion through narrow bottlenecks can be significantly slower than in the wide region; moreover, the spatial modulation of the local particle diffusivity increases with decreasing the bottleneck width. This is in clear contrast with the assumption of constant diffusivity we adopted above, when implementing the FJ-formalism and the BD simulation code. To appreciate the effect of the spatial dependence of the local diffusivity, we replace the constant diffusivity, D_0, with the experimental measurement, $D_{hyd}(x)$, reported in Fig. 4(c), both in the theoretical treatment and in the numerical code. The new analytical and numerical predictions are in plotted Fig. 2(c-f), respectively, as green curves and symbols. Their agreement with the experimental data is excellent. Furthermore, we used the improved BD code to compute, besides the first two FPT moments, also the FPT distributions displayed in Figs. 2(a, b). Again, the close comparison obtained with the experimental data confirms the validity of our phenomenological approach.

DISCUSSIONS

The coincidence of approximate analytical predictions and simulation results occurs for any choice of the local diffusivity, i.e., D_0 or $D_{hyd}(x)$, as illustrated in Fig. 2. This means that the FJ theory well describes the entropic effects of particle transport in weakly corrugated channels with $|g'(x)| < 1$ [21]. However, assuming constant particle diffusivity, as common practice in the current literature, can lead to large discrepancies between theoretical predictions and experimental observations. Indeed, to correctly analyze the diffusion of finite-size particles in narrow channels one needs to account for the hydrodynamic effects, as well. Because there is no general analytical solution for particle diffusivity in a corrugated confinement, we substituted the constant diffusivity, D_0, with an empirical function from experimental measurements, $D_{hyd}(x)$. The substitution $D_0 \to D_{hyd}(x)$ in Eq. (3), suggests a phenomenological factorization of entropic and hydrodynamic effects, whose validity is justified *a posteriori* by the reported close comparison with the experimental data. The FJ theory with hydrodynamic corrections thus remains a powerful analytical tool to investigate diffusion in complex channels.

The local diffusivity in corrugated channels displays a rich 2D structure, see Fig. 4. The comparison with a more tractable geometry helps illustrating the phenomenon of the hydrodynamic diffusivity suppression advocated above. For a spherical particle of a radius r diffusing along the axis of a relatively long cylinder [38, 47], the particle diffusivity is approximated by,

$$D \approx D_u \left[1 - 2.104\left(\frac{r}{R}\right) + 2.089\left(\frac{r}{R}\right)^3\right], \qquad (6)$$

where D_u is the particle diffusivity in an unbounded space and R denotes the cylinder radius. According to Eq. (6), particle diffusivity in confined geometries is generally smaller than in an unbounded space. In our channels, the maximum diffusivity D_0 is about 60% of the Stokes-Einstein predicted value. Diffusivity also tends to decrease as the confinement grows tighter (i.e., for larger

r/R); this explains why diffusivity is smaller in the necking regions of our channel. In certain applications, such as the entropic splitters [33], one has recourse to tight confinement to generate high entropic barriers; we expect hydrodynamically suppressed diffusion to play an important role in these situations and possibly boost the separation efficiency.

In most technological applications, particles are driven by external fields. This may prevent the system from equilibrating in the transverse directions and produce new, more complex transport mechanisms [20]. Hydrodynamics also plays a more active role in the presence of external driving [48]. Our experimental system can serve as an excellent platform to investigate these important and challenging problems.

Methods

Channel fabrication and Imaging procedure

Microchannels were fabricated with a two-photon direct laser writing system (μFAB3D from Teem Photonics). This system uses a microscope objective lens (Zeiss Fluar 100×, numerical aperture 1.3) to focus pulsed laser (Nd:YAG microchip laser with 532nm wavelength, 750ps pulse width, and 40kHz repetition rate) into a droplet of photoresist resin that is mounted on a piezo-nanopositioning stage (PI P-563.3CL). We used a polymer resin ORMOCOMP (Micro resist technology, GmbH) with a photo-initiator (1,3,5-Tris(2-(9-ethylcabazyl-3)ethylene)benzene). Photopolymerization occurs and solidifies the resin at the focal point; the piezo-stage scans the resin relative to the focal point along a preassigned trajectory [$f(x)$ in the inset of Fig. 1(a)] to fabricate the desired structure. After the scanning is finished, the remaining liquid resin was removed by washing the structure with 4-Methyl-2-pentanone and then acetone for 5 minutes. Then channels were thoroughly cleaned with distilled water to prevent particles from sticking to the channel boundaries.

Fluorescently-labeled Polystyrene particles were purchased from Invitrogen (Catalog number: F13080). Particle motion was recorded through a 60× oil objective (numerical aperture 1.3) in an inverted fluorescent microscope (Nikon Ti-E). With the help of an autofocus function (Nikon perfect focus), we imaged the diffusion of a colloidal particle in the channel for up to 20 hours at room temperature (27 °C).

Brownian dynamics simulation

The motion of a colloid particle is governed by a 2D overdamped Langevin equation in simulations. The particle diffusivity varies spatially when the diffusivity function $D_{hyd}(x)$ is used; for thermodynamic consistency, we adopted the transport (also known as kinetic or isothermal) convention [49–52] to compute the stochastic integral [49, 53]. The channel boundary was represented by a string of fixed particles, which interact with the colloidal particle via a short-range repulsive force. Particle trajectories from simulation were analyzed in the same way as their experimental counterpart to extract the effective volume of the channel's unit cell and the FPT's. See SI for more details.

Finite-element calculation

We solved the Stokes equations in a typical setup shown in Fig. S2(a). No-slip boundary conditions were imposed on the side walls, floor and ceiling, and open boundary conditions at the channel openings. The geometry of the side wall was set to reproduce the inner channel boundary measured in the experiments [see insert of Fig. 1(a)]. A sphere was driven with a constant speed, v_x, in the x direction; at different points, (x, y), on a horizontal plane. We measured the drag force, f_x, and computed the hydrodynamic drag coefficient, $\gamma(x, y) = f_x/v_x$. See SI for more details.

* hepeng_zhang@sjtu.edu.cn

[1] Hänggi, P. & Marchesoni, F. Artificial brownian motors: Controlling transport on the nanoscale. *Rev. Mod. Phys.* **81**, 387–442 (2009).

[2] Burada, P. S., Hänggi, P., Marchesoni, F., Schmid, G. & Talkner, P. Diffusion in confined geometries. *ChemPhysChem* **10**, 45–54 (2009).

[3] Berkowitz, B., Cortis, A., Dentz, M. & Scher, H. Modeling non-fickian transport in geological formations as a continuous time random walk. *Rev. Geophys.* **44**, RG2003 (2006).

[4] Kärger, J. & Ruthven, D. M. *Diffusion in Zeolites and Other Microporous Solids* (John Wiley, New York, 1992).

[5] Zhou, H.-X., Rivas, G. & Minton, A. P. Macromolecular crowding and confinement: Biochemical, biophysical, and potential physiological consequences. *Annu. Rev. Biophys.* **37**, 375–397 (2008).

[6] Bressloff, P. C. & Newby, J. M. Stochastic models of intracellular transport. *Rev. Mod. Phys.* **85**, 135–196 (2013).

[7] Deen, W. M. Hindered transport of large molecules in liquid-filled pores. *AIChE J.* **33**, 1409–1425 (1987).

[8] Benichou, O. & Voituriez, R. From first-passage times of random walks in confinement to geometry-controlled kinetics. *Phys. Rep.* **539**, 225–284 (2014).

[9] Hofling, F. & Franosch, T. Anomalous transport in the crowded world of biological cells. *Rep. Prog. Phys.* **76**, 046602 (2013).

[10] Hille, B. *Ion Channels of Excitable Membranes* (Sinauer Associates, 2001).

[11] Kettner, C., Reimann, P., Hänggi, P. & Müller, F. Drift ratchet. *Phys. Rev. E* **61**, 312–323 (2000).

[12] Matthias, S. & Müller, F. Asymmetric pores in a silicon membrane acting as massively parallel brownian ratchets. *Nature* **424**, 53–57 (2003).

[13] Wanunu, M. *et al.* Rapid electronic detection of probe-specific micrornas using thin nanopore sensors. *Nat. Nanotechnol.* **5**, 807–814 (2010).

[14] Jacobs, M. *Diffusion Processes* (Springer, New York, 1967).

[15] Zwanzig, R. Diffusion past an entropy barrier. *J. Phys. Chem.* **96**, 3926–3930 (1992).

[16] Reguera, D. & Rubi, J. M. Kinetic equations for diffusion

in the presence of entropic barriers. *Phys. Rev. E* **64**, 061106 (2001).

[17] Kalinay, P. & Percus, J. K. Corrections to the Fick-Jacobs equation. *Phys. Rev. E* **74**, 041203 (2006).

[18] Reguera, D. *et al.* Entropic transport: Kinetics, scaling, and control mechanisms. *Phys. Rev. Lett.* **96**, 130603 (2006).

[19] Berezhkovskii, A. M., Pustovoit, M. A. & Bezrukov, S. M. Diffusion in a tube of varying cross section: Numerical study of reduction to effective one-dimensional description. *J. Chem. Phys.* **126**, 134706 (2007).

[20] Burada, P. S., Schmid, G., Reguera, D., Rubi, J. M. & Hänggi, P. Biased diffusion in confined media: Test of the Fick-Jacobs approximation and validity criteria. *Phys. Rev. E* **75**, 051111 (2007).

[21] Berezhkovskii, A. M., Dagdug, L. & Bezrukov, S. M. Range of applicability of modified Fick-Jacobs equation in two dimensions. *J. Chem. Phys.* **143**, 164102 (2015).

[22] Ai, B. Q. & Liu, L. G. Current in a three-dimensional periodic tube with unbiased forces. *Phys. Rev. E* **74**, 051114 (2006).

[23] Dagdug, L., Berezhkovskii, A. M., Makhnovskii, Y. A., Zitserman, V. Y. & Bezrukov, S. M. Communication: Turnover behavior of effective mobility in a tube with periodic entropy potential. *J. Chem. Phys.* **134**, 101102 (2011).

[24] Borromeo, M. & Marchesoni, F. Particle transport in a two-dimensional septate channel. *Chem. Phys.* **375**, 536–539 (2010).

[25] Bradley, R. M. Diffusion in a two-dimensional channel with curved midline and varying width: Reduction to an effective one-dimensional description. *Phys. Rev. E* **80**, 061142 (2009).

[26] Dagdug, L. & Pineda, I. Projection of two-dimensional diffusion in a curved midline and narrow varying width channel onto the longitudinal dimension. *J. Chem. Phys.* **137**, 024107 (2012).

[27] Bauer, M., Godec, A. & Metzler, R. Diffusion of finite-size particles in two-dimensional channels with random wall configurations. *Phys. Chem. Chem. Phys.* **16**, 6118–6128 (2014).

[28] Burada, P. S. *et al.* Entropic stochastic resonance. *Phys. Rev. Lett.* **101**, 130602 (2008).

[29] Ding, H., Jiang, H. J. & Hou, Z. H. Entropic stochastic resonance without external force in oscillatory confined space. *J. Chem. Phys.* **142**, 194109 (2015).

[30] Hänggi, P., Marchesoni, F., Savelèv, S. & Schmid, G. Asymmetry in shape causing absolute negative mobility. *Phys. Rev. E* **82**, 041121 (2010).

[31] Marchesoni, F. & Savelèv, S. Rectification currents in two-dimensional artificial channels. *Phys. Rev. E* **80**, 011120 (2009).

[32] Malgaretti, P., Pagonabarraga, I. & Rubi, J. M. Confined brownian ratchets. *J. Chem. Phys.* **138**, 194906 (2013).

[33] Reguera, D. *et al.* Entropic splitter for particle separation. *Phys. Rev. Lett.* **108**, 020604 (2012).

[34] Marquet, C., Buguin, A., Talini, L. & Silberzan, P. Rectified motion of colloids in asymmetrically structured channels. *Phys. Rev. Lett.* **88**, 168301 (2002).

[35] Huang, L. R., Cox, E. C., Austin, R. H. & Sturm, J. C. Continuous particle separation through deterministic lateral displacement. *Science* **304**, 987–990 (2004).

[36] Mathwig, K., Müller, F. & Gösele, U. Particle transport in asymmetrically modulated pores. *New J. Phys.* **13**, 033038 (2011).

[37] Pagliara, S. *et al.* Diffusion coefficients and particle transport in synthetic membrane channels. *Eur. Phys. J.: Spec. Top.* **223**, 3145–3163 (2014).

[38] Happel, J. & Brenner, H. *Low Reynolds Number Hydrodynamics* (Prentice Hall, Englewood Cliffs, NJ, 1965).

[39] Volpe, G., Helden, L., Brettschneider, T., Wehr, J. & Bechinger, C. Influence of noise on force measurements. *Phys. Rev. Lett.* **104**, 170602 (2010).

[40] Chen, S. B. Drag force of a particle moving axisymmetrically in open or closed cavities. *J. Chem. Phys.* **135**, 014904 (2011).

[41] Dettmer, S. L., Pagliara, S., Misiunas, K. & Keyser, U. F. Anisotropic diffusion of spherical particles in closely confining microchannels. *Phys. Rev. E* **89**, 062305 (2014).

[42] Skaug, M. J., Wang, L., Ding, Y. F. & Schwartz, D. K. Hindered nanoparticle diffusion and void accessibility in a three-dimensional porous medium. *ACS Nano* **9**, 2148–2156 (2015).

[43] Goel, N. S. & Richter-Dyn, N. *Stochastic Models in Biology* (Academic Press Inc, New York, 1974).

[44] Hänggi, P., Talkner, P. & Borkovec, M. Reaction-rate theory: fifty years after kramers. *Rev. Mod. Phys.* **62**, 251–341 (1990).

[45] Eral, H. B., Oh, J. M., van den Ende, D., Mugele, F. & Duits, M. H. G. Anisotropic and hindered diffusion of colloidal particles in a closed cylinder. *Langmuir* **26**, 16722–16729 (2010).

[46] Cervantes-Martinez, A. E., Ramirez-Saito, A., Armenta-Calderon, R., Ojeda-Lopez, M. A. & Arauz-Lara, J. L. Colloidal diffusion inside a spherical cell. *Phys. Rev. E* **83**, 030402 (2011).

[47] Misiunas, K., Pagliara, S., Lauga, E., Lister, J. R. & Keyser, U. F. Nondecaying hydrodynamic interactions along narrow channels. *Phys. Rev. Lett.* **115**, 038301 (2015).

[48] Martens, S., Straube, A. V., Schmid, G., Schimansky-Geier, L. & Hänggi, P. Hydrodynamically enforced entropic trapping of Brownian particles. *Phys. Rev. Lett.* **110**, 010601 (2013).

[49] Hänggi, P. Stochastic processes. i. asymptotic behaviour and symmetries. *Helv. Phys. Acta* **51**, 183–201 (1978).

[50] Sokolov, I. M. Itô, Stratonovich, Hänggi and all the rest: The thermodynamics of interpretation. *Chem. Phys.* **375**, 359–363 (2010).

[51] Farago, O. & Gronbech-Jensen, N. Langevin dynamics in inhomogeneous media: Re- examining the ito-stratonovich dilemma. *Phys. Rev. E* **89**, 013301 (2014).

[52] Bruti-Liberati, N. & Platen, E. Strong predictor–corrector Euler methods for stochastic differential equations. *Stochastics and Dynamics* **8**, 561–581 (2008).

[53] van Kampen, N. G. Itô versus Stratonovich. *J. Stat. Phys.* **24**, 175–187 (1981).